Earth, Planets and Space

EXPRESS LETTER

Open Access

The probable direction of impact at Dhala impact structure, India deciphered from microfracture intensity and X-ray diffractometry: a new potential impact direction indicator

Swastik Suman Behera[1], Sonal Tiwari[1], Ambrish Kumar Pandey[1], Amar Agarwal[1*] and Arun Kumar Ojha[2]

Abstract

The most widely used method of determining impact direction employs asymmetric ejecta distribution around the crater. However, the active terrestrial landscape seldom preserves the pristine ejecta blanket, making it challenging for this analysis to be carried out. The deeply eroded Dhala impact structure, formed during the Proterozoic, is devoid of an ejecta blanket. We, therefore, utilize the variation in the full width at half maxima (FWHM) of the quartz (100) peak in X-ray diffraction (XRD) spectra and the P_{10} microfracture intensity in the monomict breccia to estimate the probable downrange direction of the Dhala impact structure. The monomict breccia rocks of the Dhala impact structure have experienced low shock pressures (< 10 GPa) and are highly fractured, making them the ideal target lithology for our study. Previous studies have used XRD extensively for strain analysis in synthetic materials and rocks. Microfracture intensity acts as an indicator for the degree of fracturing or brittle damage in the rocks, with the maximum shock-induced damage being concentrated in the downrange direction. The results from the XRD are consistent with the microfracture intensity analyses and indicate that the probable direction of impact was from southwest to northeast, with northeast being the downrange direction. Furthermore, we suggest that the degree of fracturing and X-ray diffractometry can be used to identify the downrange direction of an impact crater.

Keywords Dhala Impact structure, shock induced microfractures, X-ray Diffractometry, shock barometry from XRD, impact direction

*Correspondence:
Amar Agarwal
amar@daad-alumni.de
Full list of author information is available at the end of the article

Graphical Abstract

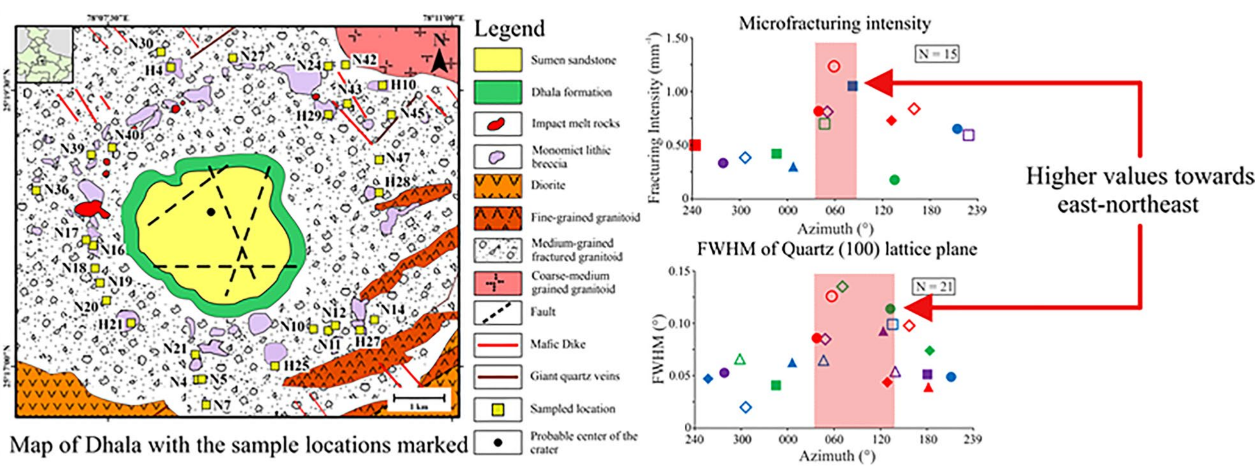

Introduction

For planetary impacts, the obliquity and direction of impact play a pivotal role in defining the shape of the crater and the central uplift, the distribution of ejecta, the size of the crater, the final state of the projectile, the decay of shock pressure, the amount of shock melting and the ejection of matter from planetary surfaces to name a few (Gault and Wedekind 1978; Pierazzo and Melosh 2000a; Kenkmann et al. 2020; Sugandhi and Agarwal 2022; Sugandhi et al. 2024). Hence, characterizing the direction of impact is a crucial aspect of the study of impact craters. Theoretical studies have established that oblique impacts are more likely than vertical ones (Gilbert 1893; Pierazzo and Melosh 2000a).

Actual progress in understanding the effect of obliquity, i.e., changes in parameters with respect to uprange and downrange direction, has been made possible with recent advancements in numerical and 3D simulations and with the feasibility of carrying out hypervelocity impact experiments (Burcheil and Mackay 1998; Pierazzo and Melosh 1999, 2000a, b; Dahl and Schultz 2001; Heineck et al. 2002; Anderson et al. 2003, 2004; Elbeshausen et al. 2009; Davison et al. 2011; Shuvalov 2011; Michikami et al. 2017; Collins et al. 2020; Davison and Collins 2022). The easiest identifier of the direction of impact is the distribution of ejecta, for example, the bi-lateral symmetric ejecta distribution around a crater, with ejecta extending further in the downrange direction in low-oblique impacts, and concentrated crossrange in highly oblique impacts (Gault and Wedekind 1978). However, the active geologic landscape of the Earth poses a major challenge to the identification of terrestrial oblique impact craters as the ejecta blanket gets eroded over time. The scope of identifying the direction of impact by the crater shape is low, as despite oblique impacts being more likely, most of the documented planetary craters are circular in nature (Pierazzo and Melosh 2000a; Elbeshausen et al. 2013). Only for highly oblique impacts (impact angle < 15°), the crater is elongated in the direction of impact (Gault and Wedekind 1978; Bottke et al. 2000). This necessitates other tools.

During the initial contact of a projectile with the ground, shock waves are generated which move outward from the point of impact. The propagation of shock waves through a medium causes an irreversible deformation known as shock metamorphism (Ahrens and Rosenberg 1968; Stöffler et al. 1975; Langenhorst et al. 1992; Stöffler and Langenhorst 1994). Fractures associated with the impact form at different stages during the propagation of the shock waves (Kenkmann et al. 2014). These can generally be classified into (i) radial, (ii) concentric, and (iii) spall fractures (Field 1971; Ahrens and Rubin 1993). While the radial fractures develop during the compressive phase of the shock wave, the concentric fractures develop during the release phase (Agarwal et al. 2015, 2016, 2017). Numerical simulations carried out to study oblique impacts indicate that most of the shock pressure is concentrated in the downrange direction (Pierazzo and Melosh 2000a). These results are backed up by cratering experiments which show that the magnitude of peak stress and the shock-induced damage is higher in the downrange as compared to the uprange direction (Schultz and Anderson 1996; Dahl and Schultz 2001; Ai and Ahrens 2005).

X-ray diffractometry (XRD) is extensively used to determine material properties like crystal structure, crystallite size, and lattice strain. The nature of the lattice strain is determined by the shifting of a peak, characterized by a change in the 2θ angle (peak position), and the broadening of a peak, determined by variation in the full width at half maxima (FWHM) (Williamson and Hall 1953; Ungár 2004). FWHM is generally used as an indicator of strain with higher FWHM indicating higher strain in rocks (Williamson and Hall 1953; Nasiri-Tabrizi 2014). Peak shifting indicates uniform strain whereas peak broadening indicates non-uniform strain. In synthetic materials, XRD has been extensively used not just to study peak shifting and broadening but also for the calculation of particle size and strain (Khorsand Zak et al. 2012; Thandavan et al. 2015; Kibasomba et al. 2018; Wu et al. 2019). Though rare, XRD has been used to carry out similar studies in natural rocks and minerals as well (Reznik et al. 2016; Agarwal and Alva-Valdivia 2019; Kumar et al. 2023). Kumar et al. (2023) reported an increase in the FWHM of the quartz (011) peak with increasing strain rate and Reznik et al. (2016) documented an increase in FWHM in magnetite with increasing shock pressure, at low shock pressures.

The Dhala impact structure is more than 1.7 Ga old and is a deeply eroded structure (Pati et al. 2008). The lack of a preserved ejecta blanket and the presence of syn- to postimpact sediments over a significant part of the structure makes it difficult to employ the conventional methods of identification of oblique impact craters. Hence, we turn to the two aforementioned laboratory techniques (degree of fracturing and XRD) to look for evidence of an oblique impact and to estimate the probable direction of the impact.

Geologic setting

Located nearly 50 km west of Jhansi city, the Dhala impact structure (Fig. 1) is almost 11 km in diameter (Fig. 1) and occupies an area of nearly 64 km^2 (Pati et al. 2008, 2019). Initially thought of as a “crypto-volcanic explosion” structure (Basu 1986), the presence of shock planar deformation features (Pati et al. 2008) proved the meteoritic impact origin of the Dhala structure. The Bundelkhand craton forms the target basement of the impact structure. The Bundelkhand craton is one of the five Archean cratons of the Indian subcontinent. With an estimated areal extent of almost 29,000 km^2, the Bundelkhand craton is dominantly composed of the older tonalite–trondhjemite–granodiorite (TTG) gneisses intruded by younger granitoids and granodiorites (Pati et al. 2019; Deb and Bhattacharyya 2022). In addition, meta-sediments of Banded Iron Formations, felsic volcanics, calc–silicate rocks, amphibolites, corundum-bearing schists, and quartzites are also present (Mondal et al. 2002; Malviya et al. 2006; Pati et al. 2010; Saha et al. 2011). Collectively, they are known as the Bundelkhand Granitoid Complex. Three tectonic events between 3.3 and 2.4 Ga have deformed the TTG gneisses and the meta-sediments. The younger granitoids are further classified as medium-to-fine-grained and coarse-grained. The darker medium-to-fine-grained granitoids are composed of alkali feldspar, quartz, plagioclase, muscovite, hornblende, biotite, zircon, magnetite, chlorite, and epidote. The porphyritic coarse-grained granitoids are dominantly composed of quartz, plagioclase, alkali feldspar, hornblende, biotite, and chlorite. NNE–SSW trending giant quartz veins crosscut by NW–SE trending tholeiitic mafic dike swarms are also present throughout the craton (Pati et al. 2010).

At Dhala, the impactite lithologies consist of suevites, pseudotachylitic breccias, monomict breccias, and impact melt rocks. The bottommost layer, suevite is composed of lithic and melt clasts imbedded in a fine-grained matrix composed of shocked lithic and mineral clasts and glassy or crystalline impact melt (Pati et al. 2019). The pseudotachylite breccias (PTBs) occur as veins in the host granitoids. Within the PTBs, the lithic clasts are more abundant than the mineral clasts and the matrix of the PTBs can be extremely fine-grained, rich in phyllosilicates (chlorite, biotite, and sericite), or may contain melt components. The PTBs are further classified into the light grey colored cataclastic PTBs and the dark grey to black colored melt-bearing PTBs. The clasts of cataclastic PTBs are highly angular and do not show significant alteration whereas the melt-bearing PTBs are highly altered (Pati et al. 2015). Impact melt rocks are reddish orange in color with elliptical vesicles and amygdales on their surface. They are composed of clasts containing feldspars, quartz, biotite, magnetite, ilmenite, and zircons and indicate significant post-impact hydrothermal alterations (Pati et al. 2010, 2019; Joshi et al. 2023). The presence of planar deformation features and feather features in shocked quartz grains indicate shock pressures of ~ 20–25 GPa, while the presence of zircon grains and diaplectic glass indicate shock pressures as high as 60 GPa (Pati et al. 2019). Thus, the impact melt rocks likely experienced shock pressures between 20 and 60 GPa.

Monomict breccia is generally autochthonous and forms during the excavation stage of crater formation in the proximal ejecta blanket close to the wall of the transient cavity or the fractured basement rocks of the crater (Kenkmann et al. 2014). In Dhala, the reddish-brown, whaleback-like elevated outcrops of monomict breccia consist of extensively fractured and brecciated coarse-to-medium grained granitoid and form the outermost ring

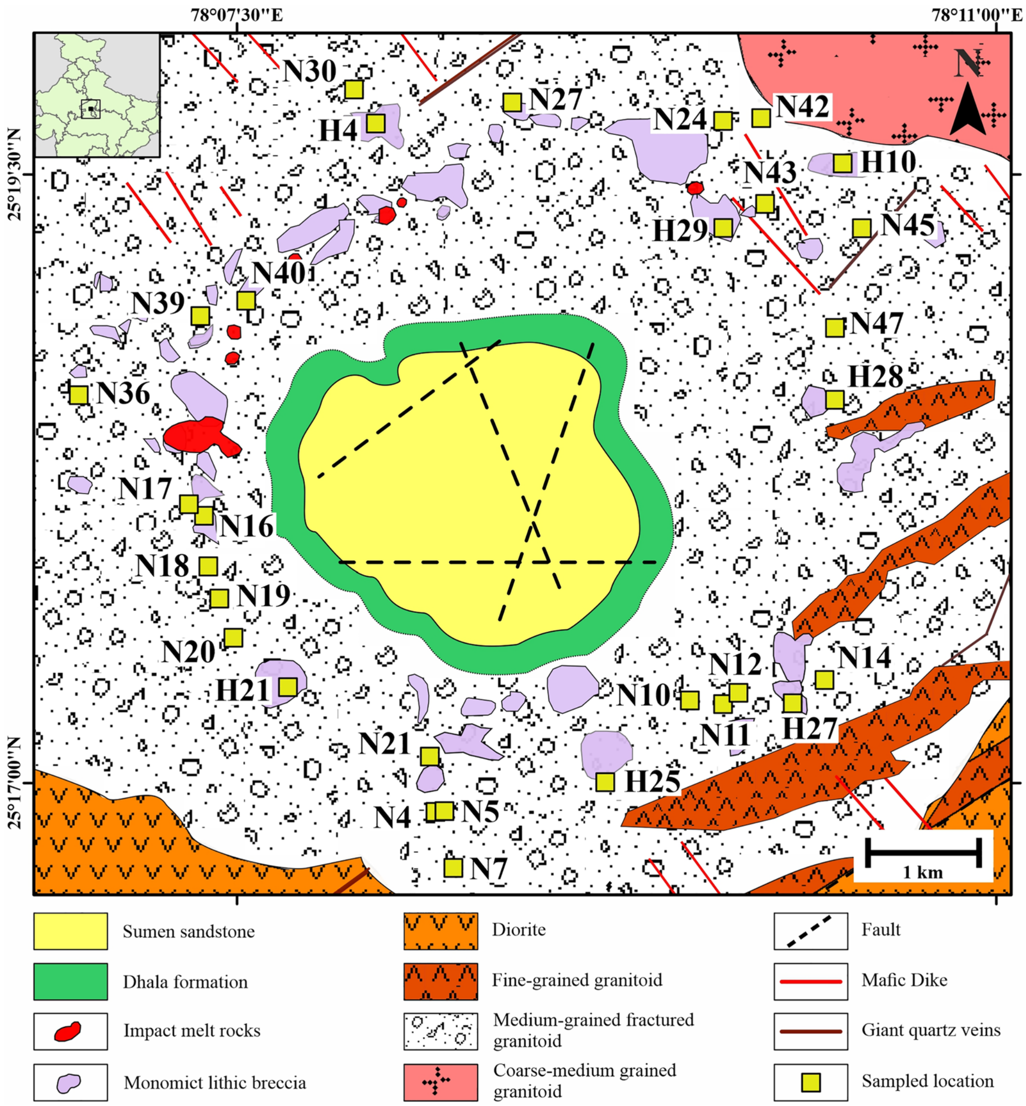

Fig. 1 Geologic map of the Dhala impact structure showing major lithologies and sample locations (modified after Singh et al. 2021)

of the Dhala structure. They are generally composed of clasts of K-feldspar and quartz in a feldspar-rich matrix; the clasts are pervaded by trans-granular microfractures filled with impact melt. Pati et al. (2019) reported a shatter cone in the northeastern outcrops of monomict breccia indicating shock pressure less than 10 GPa.

The impactite lithologies were overlain by rocks of the Dhala formation, which are stratigraphically equivalent to the Semri Group of the Vindhyan supergroup (Pati et al. 2019). The Dhala formation is a layer of post-impactite sediments composed of sandstones, siltstones, shales, and conglomerates. These sediments are dominantly composed of poorly sorted, angular clasts of quartz, feldspars, biotite, and sericite in a feldspar and sericite-rich matrix (Agarwal et al. 2020). The central elevated area (CEA) is a ~ 418 m tall mesa-like structure that unconformably overlies the rocks of the Dhala formation. It is almost 5 km^2 in area and is composed of Sumen sandstone of the Kaimur group in the Vindhyan supergroup. The presence of a scarce amount of shocked quartz grains in the CEA indicates the reworking and deposition of the ejecta blanket by postimpact processes to form the CEA (Agarwal et al. 2020). The age of the Vindhyan supergroup has been calculated as 1.7 ± 0.11 Ga., by the

Pb–Pb whole-rock technique (Sarangi et al. 2004). This also serves as the minimum age limit for the Dhala impact event.

Methodology

For this study, we collected thirty hand samples of monomict breccia oriented in the field with a magnetic compass. Oriented thin sections were prepared from each hand sample for X-ray diffraction (XRD) analysis and microfracture intensity study. The thin sections were analyzed and photographed under plane and cross-polarized light using an optical scanning microscope, Leica DM4. For each of these thin sections, the P_{10} microfracture intensity was calculated. P_{10} is one of the methods within the P_{ij} system of microfracture intensity measurements (Dershowitz and Herda 1993), commonly used by the Discrete Fracture Network modeling community (Rogers et al. 2017; Tonkins and Coggan 2017; Lei et al. 2017). P_{10} is a linear measure of fracture intensity. It is given as the number of fractures per unit length of scan lines. We calculated the number of intersections between the microfractures and scan lines and the total length of the scan lines within the clasts (Supp. Table 1). The intensity was calculated as

$$P10\left(mm^{-1}\right) = \frac{Number\ of\ inter\ sections\ between\ microfractures\ and\ scan-lines}{Total\ length\ of\ the\ scan-lines\ within\ the\ clasts(mm)}$$

The scan lines required in this method were constructed in the ArcGIS Pro desktop software. A mesh of two mutually perpendicular sets of scan lines, with 1 mm line spacing, was constructed over the entire thin section image (Supp. Figure 1). The microfracture intensity was calculated for all the thin sections and the variation in the microfracture intensity values with the azimuth was plotted. Only fractures present within the clasts were considered.

The XRD analysis of the samples was carried out with a PANalytical X'Pert Pro diffractometer housed in the Advanced Center for Material Sciences at the Indian Institute of Technology, Kanpur. The 2θ angle was varied between 5° and 70° at an angular speed of 0.1°/sec to generate the XRD spectra, which were then analyzed in the Origin Pro software. To calculate the full width at half maxima (FWHM) and the peak position (2θ) a Gaussian curve (Williamson and Hall 1953) was fitted on each peak in the XRD spectra (Supp. Figure 2). With the help of the X'Pert Highscore Plus 3.0 software, the 2θ values were used to identify the lattice planes of the minerals.

The application of the proposed method warrants certain precautions. First, it is only effective in impactite lithologies that have experienced shock pressures < 20 GPa. At shock pressures over 20 GPa, the formation of fractures is no longer the preferred mechanism of deformation, and localized amorphization of rocks takes place (Kenkmann et al. 2014). Low shock pressure regions can be identified in the field by the presence of shatter cones (~1–10 GPa), and under a microscope by the presence of planar fractures (~5–10 GPa), feather features, and planar deformation features (~5–35 GPa) within the mineral grains (Kenkmann et al. 2014). Second, the collected rock samples should be almost equidistant from the estimated point of impact. With increasing distance from the point of impact, the amount of brittle deformation (Buhl et al. 2013b, a, 2014) as well as the FWHM of the peaks in the XRD spectra (Agarwal and Alva-Valdivia 2019) decreases. Third, the rock should be autochthonous or parautochthonous. Rocks that have suffered significant displacement may not be true indicators of the direction and distance with respect to the estimated point of impact. Fourth, the pre- and post-impact tectonic activity in the study area should be well-characterized. Tectonic activity can introduce new fractures as well as strain in the samples leading to an overestimation in the fracturing intensity and FWHM values and fifth, the samples should be evenly distributed around the estimated point of impact. Missing samples would lead to gaps in our data which might lead to errors in the estimation of the direction of impact.

To appreciate the variation in microfracture intensity and XRD data around the impact structure, the bearing of the sample locations with respect to a reference point was needed. We fitted a circle through the maximum outer extents of the monomict breccia (Supp. Figure 3). The center of this circle was regarded as the probable point of impact. The angle subtended from the North (in degrees), by each sample location on this estimated point of impact was calculated.

Results

Petrographic analysis

The monomict breccia are highly fractured, with angular clasts, which are surrounded by a very fine-grained matrix or by glassy textured impact melt (Fig. 2d). The impact melt also fills some of the microfractures (Fig. 2e). Feldspars, namely plagioclase and orthoclase and quartz are the dominant minerals both within the clasts and the fine-grained matrix. The size of the quartz grains can range from very fine-grained to almost 1500 μm, while the feldspar grains can be as large as 1800 μm. The modal

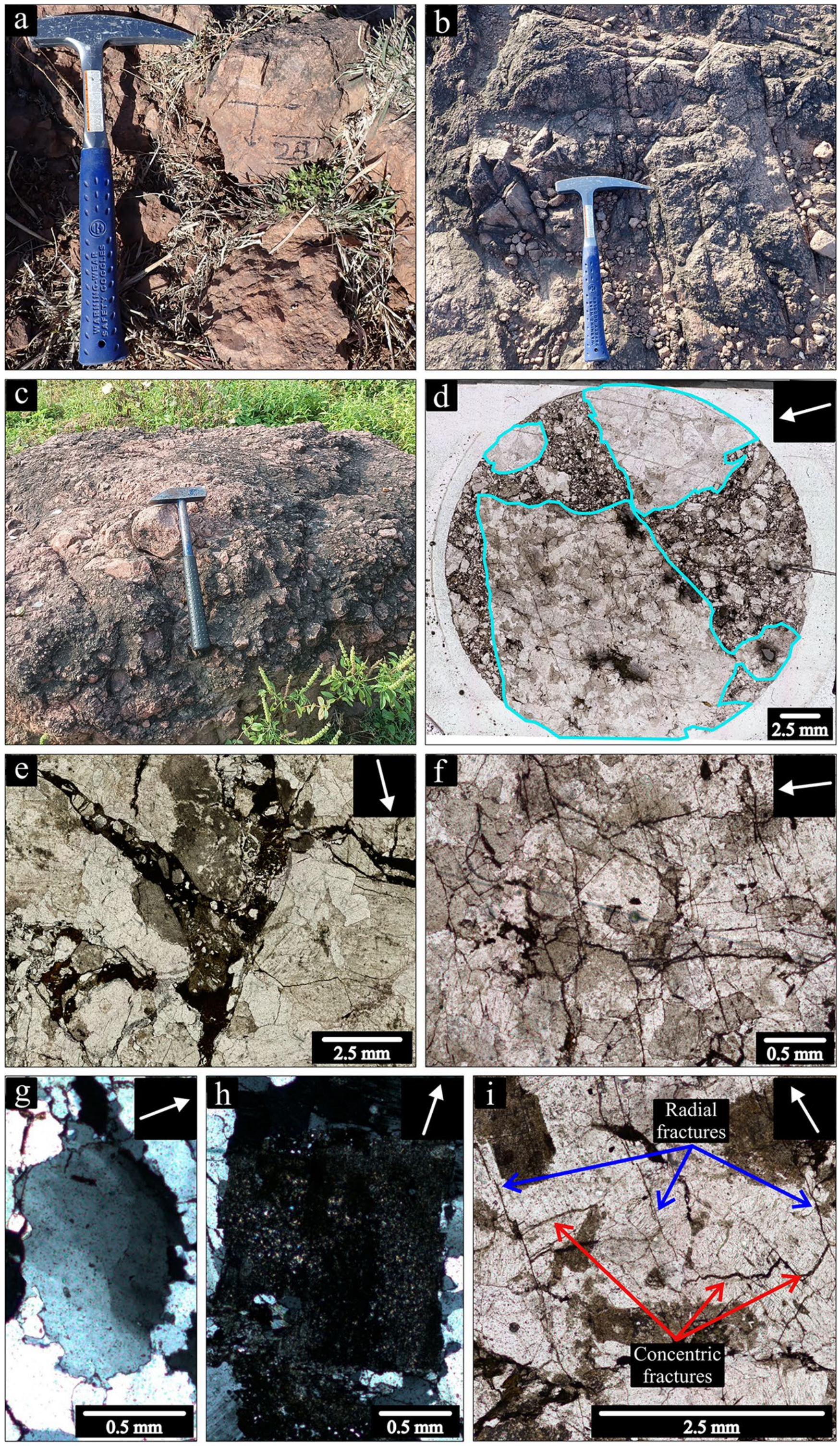

Fig. 2 **a** Oriented block of monomict breccia (H28) collected from the field. **b**, **c** Outcrops of monomict breccia in the field. A thin section under plane-polarized light showing **d** different clasts embedded in the finer matrix and **e** melt filling the space between clasts and **f** multiple microfractures within the clasts. A thin section under cross-polarized light showing **g** pre-impact undulose extinction and serrated grain boundaries in quartz and **h** sericitization in K-feldspar. **i** Cross-cutting relationships showing the concentric fractures terminating against the radial fractures. **c–g** White arrow within the black inset at the top-right points towards the estimated point of impact

percentage ratio of feldspars to quartz within the clasts varies between 60:30 and 40:50, while minerals such as chlorite, biotite, zircon, apatite, rutile, and opaque minerals make up the remaining 10% of the composition (Fig. 2). Within the clasts, most of the mineral grains have a euhedral-to-subhedral shape. Pre-impact tectonic deformation at high P–T conditions is realized as undulose extinction and serrated grain boundary in quartz grains (Fig. 2g). There are three stages of pre-impact deformation reported from the area (Prasad et al. 1999; Bhatt and Singh 2011; Deb and Bhattacharyya 2022). Post-impact hydrothermal alteration in some samples (Pati et al. 2008; Singh et al. 2021) is evidenced by sericitization of the plagioclase feldspar grains (Fig. 2h).

Microfracture intensity

Most of the clasts are pervaded by high aspect-ratio opening-mode microfractures having lengths between 1 and 10 mm and apertures between 0.01 and 0.04 mm. The traces of the microfractures are generally curvilinear or straight and they either trend radially outwards from the point of impact, parallel to the crater rim, i.e., concentric, or have a random orientation. Based on the orientation of the thin sections, most of the microfractures can be classified as radial or concentric fractures. The cross-cutting relationships indicate that the radial fractures formed earlier than the concentric fractures (Fig. 2i). In the investigated fifteen samples, the microfracture intensity varies between 1.23 and 0.17 mm^{-1} (Fig. 3a). It averages at 0.64 mm^{-1} with and standard deviation of 0.29 mm^{-1}. The intensity is lowest in sample no. N12 and highest in sample no. N45 (Fig. 3a, Supp. table 1). In general, the microfracture intensity is highest in samples from ENE and lower in samples collected from other parts of the impact structure (Fig. 3a).

XRD analysis

The X-ray diffraction spectra of the samples are dominated by signatures of the lattice planes of quartz (Supp. Table 2). Multiple lattice planes of quartz including (100), (101), (211), (212), (110), (102), (200), (201), (112), and (202) have been identified in the samples. Not all these planes have a high intensity or can be identified relatively easily in the XRD plots of all thirty samples (Supp. Figure 4). Thus, the variation in FWHM of only quartz (100) peak, identified in 21 samples, and quartz (101) peak, identified in 27 samples were considered.

The FWHM value of quartz (100) peak varies between 0.02° and 0.14° and it averages at 0.07° with and standard deviation of 0.03°. The intensity is lowest in sample no N40 and highest in sample no. N47 (Fig. 3b, Supp. Table 2). The FWHM value of quartz (101) peak varies between 0.03° and 0.13° (Fig. 3c). It averages at 0.05° with

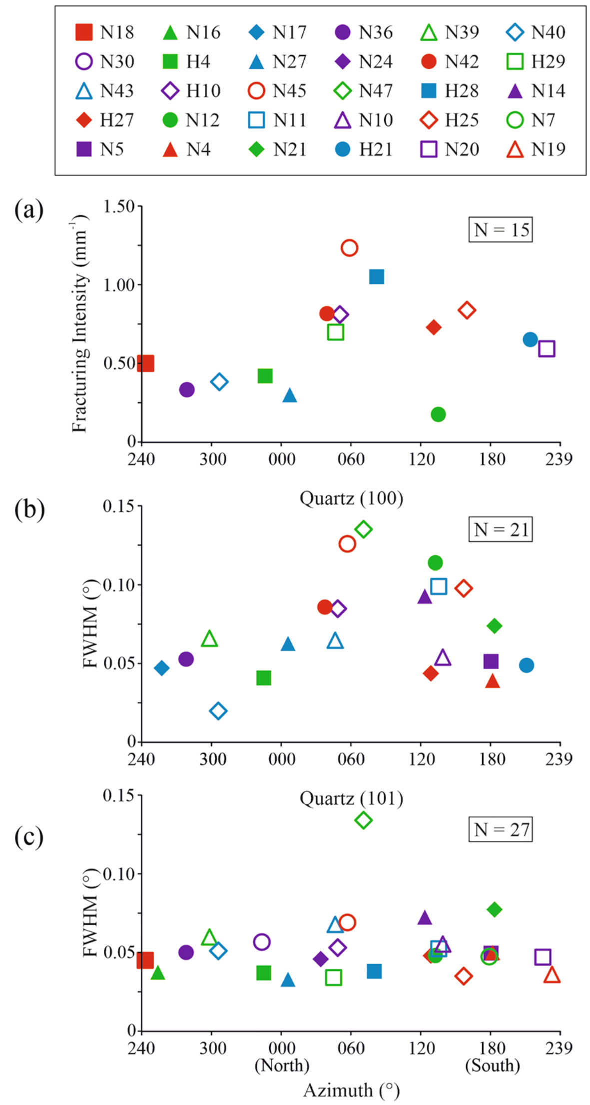

Fig. 3 Variation in the **a** P_{10} microfracture intensity, **b** FWHM of quartz (100) peak, **c** FWHM of quartz (101) peak around the estimated point of impact. The *x*-axis shows the bearing of the sample locations from the estimated point of impact

and standard deviation of 0.02°. The intensity is lowest in sample no. N27 and highest in sample no. N47 (Fig. 3c, Supp. Table 2). For the quartz (100), peak the highest FWHM values are observed in samples collected from ENE (~070°), while the FWHM of the quartz (101) peak does not show any trend (Fig. 3b, c).

Discussion

The highest intensity fracturing, P_{10} values, are recorded in samples from the ENE, ~060° (Fig. 3a). The brittle deformation at the microscopic scale is, therefore, highest in the ENE. On moving away from this direction, the intensities of fracturing and, thus, the brittle deformation decreases. More intense deformation in ENE may have been caused by a stronger shock in this direction. Concurring trends are observed in the XRD spectra with higher FWHM values of Quartz (100) peak towards the ENE (~70°) from the probable point of impact.

However, we do not see any discernible trend in the variation of the FWHM values of quartz (101) peak (Fig. 3c). It is possible that the deformation intensity or mechanism varies across the different lattice planes of quartz as previous studies have indicated that planar deformation features (PDFs) and planar fractures in shocked quartz have a preferential distribution along certain lattice planes (Goltrant et al. 1992; Stöffler et al. 2017). This has been observed in the Dhala impact structure as well (Pati et al. 2019).

The Bundelkhand granitoid and the Dhala impact structure have a significant post-impact geologic history, including the emplacement of the Dhala formation and Sumen sandstone, three distinct phases of hydrothermal activity, and the intrusion of mafic dykes (Pati et al. 2015, 2019; Agarwal et al. 2020; Singh et al. 2021; Joshi et al. 2023). Furthermore, evidence of post-impact fracturing and fluvial and glacial activity has also been reported from the area (Singh et al. 2021). While this may have affected our estimation of the P_{10} fracturing intensity, most of the measured microfractures could be classified as radial and concentric, thus indicating their impact origin (Fig. 2). Furthermore, although it has been established with relative certainty that higher degrees of fracturing can cause enhanced rates of weathering (Molnar et al. 2007; Roy et al. 2015, 2016; Duvall et al. 2020), the converse is not so well-established. Thus, it is not possible to separate out the effect of weathering and hydrothermal activity from our estimated fracture intensity values. In addition, necessary precautions were taken during sampling to avoid collecting weathered samples.

Notably, a trend similar to that of the fracture intensity values is also indicated by the FWHM values of Quartz (100) peaks. Quartz is highly resistant to both mechanical and physical weathering (Gerrard 1988; Nesse 2017), thus its XRD peaks are unlikely to be significantly affected by weathering processes. While quartz is still susceptible to hydrothermal alterations (Monecke et al. 2002), the samples selected for this study were not collected from the alteration halo, which, at Dhala is located in the immediate proximity of the Giant Quartz Veins. Thus, we argue that the effect of hydrothermal alteration on the fracture intensity and quartz FWHM was minimal. This argument is supported by the presence of unaltered grains of quartz and magnetite (highly susceptible to alteration) in some of the collected samples (Supp. Figure 6).

Several authors have previously attempted to evaluate the direction as well as the angle of impact in terrestrial craters from the crater morphology by integrating experimental, field, and remote sensing observations (Schultz and Anderson 1996; Schultz and D'Hondt 1996; Shoemaker and Shoemaker 1996; Ekholm and Melosh 2001; Stöffler et al. 2002; Herrick and Forsberg-Taylor 2003; Kenkmann et al. 2005; Lindström et al. 2005; Tsikalas 2005; Wallis et al. 2005; Poelchau and Kenkmann 2008). These methods are, however, difficult to apply to the deeply eroded Dhala impact structure whose morphology is not preserved and is also overlain by post-impact sedimentary layers. In this study, we propose a new method which integrates field and micro-scale observations from the impactite lithologies with previous experimental studies to estimate the direction of impact. The accuracy of this method cannot be commented upon as of right now as there are no other studies estimating the direction of impact at the Dhala impact structure. However, we propose that this method, which is yet to be verified, can be applied to various pristine and eroded craters meeting the criteria laid down in the Methodology section.

3-D numerical models for oblique impacts indicate that although the propagation of shock waves in the target rock is symmetric, the strength of the shock waves is asymmetric with the strongest waves concentrated in the downrange direction (Pierazzo and Melosh 1999, 2000a). These results have been backed up by cratering experiments which report higher shock-induced damage beneath craters in the downrange as compared to the uprange direction (Ai and Ahrens 2005). Furthermore, experiments measuring the stress wave asymmetry in oblique impacts indicate that in target rocks downrange, the peak stress is almost twice the peak stress in the uprange direction (Dahl and Schultz 2001). This higher peak stress also suggests a higher damage in the downrange direction.

Conclusions

In this study, we have calculated the FWHM of quartz and microfracture intensity in the monomict breccia of the Dhala impact structure. While the FWHM is an indicator of lattice strain, the microfracture intensity has a positive correlation with the shock-induced brittle damage. Thus, we propose that fracturing intensity and FWHM of a mineral peak from XRD data can be used as a viable tool to understand the distribution of damage around an impact crater. Since, in inclined impacts, higher damage is focused in the downrange, we suggest that fracturing intensity and FWHM can be used to identify the downrange direction of a crater. In our study, the monomict breccia outcrops located towards the northeast from the calculated point of impact show the highest values of fracturing intensity as well as FWHM of quartz. Hence, we suggest that northeast is the probable downrange and the direction of impact at the Dhala impact structure was possibly from southwest to northeast.

Supplementary Information

The online version contains supplementary material available at https://doi.org/10.1186/s40623-024-02028-1.

Supplementary material 1.

Supplementary material 2.

Supplementary material 3.

Acknowledgements

SSB thanks IIT Kanpur for fellowship. AA acknowledges the financial support from IITK/ES/2019372 (IIT Kanpur, India), NCPOR/IODP/E.3947/2021 (NCPOR, MoES) and the Alexander von Humboldt research group linkage program. The authors would like to thank the two anonymous reviewers and Dr Takeshi Sagiya (Editor-in-Chief) for their comments which have significantly improved the quality and readability of the manuscript.

Author Contributions

SSB carried out the sample collection, data acquisition and analysis, interpretation of the results, and the preparation of the original draft of the manuscript. ST helped with the data analysis and the interpretation of the results. AKP helped with the sample collection and preparation, and data acquisition. AA conceptualized, designed, and supervised the project, and helped with the interpretation of the results and the preparation of the original draft. AKO helped with the project design and the preparation of the original draft. All authors read and approved the final manuscript.

Competing Interests

The authors declare that they have no competing interests.

Author details

[1]Applied Structure Geology Group, Department of Earth Science, Indian Institute of Technology Kanpur, Kanpur 47667, Uttar Pradesh, India. [2]CSIR-National Geophysical Research Institute, Hyderabad 500007, India.

Received: 20 January 2024 Accepted: 15 May 2024
Published online: 11 June 2024

References

Agarwal A, Alva-Valdivia LM (2019) Curie temperature of weakly shocked target basalts at the Lonar impact crate. Earth Planets Space India. https://doi.org/10.1186/s40623-019-1120-9

Agarwal A, Kontny A, Greiling RO (2015) Relationships among magnetic fabrics, microfractures and shock pressures at an impact crater: a case study from Lockne crater, Sweden. J Appl Geophy 114:232–243. https://doi.org/10.1016/J.JAPPGEO.2015.01.010

Agarwal A, Kontny A, Srivastava DC, Greiling RO (2016) Shock pressure estimates in target basalts of a pristine crater: a case study in the lonar crater, India. Bull Geol Soc Am 128:19–28. https://doi.org/10.1130/B31172.1

Agarwal A, Reznik B, Srivastava DC (2017) Alternating augite-plagioclase wedges in basement dolerites of Lockne impact structure, Sweden : a new shock wave-induced deformation feature. Meteorit Planet Sci 470:458–470. https://doi.org/10.1111/maps.12806

Agarwal A, Kumar S, Joshi G, Agarwal KK (2020) Evidence for shock provides insight into the formation of the central elevated area in the Dhala impact structure, India. Meteorit Planet Sci 55:2772–2779. https://doi.org/10.1111/maps.13604

Ahrens TJ, Rosenberg JT (1968) Shock metamorphism: Experiments on quartz and plagioclase. In: French BM, Short NM (eds) Shock metamorphism of Natural Minerals. Mono Book Corporation, pp 59–81

Ahrens TJ, Rubin AM (1993) Impact-induced tensional failure in rock. J Geophys Res Planets 98:1185–1203. https://doi.org/10.1029/92JE02679

Ai H-A, Ahrens TJ (2005) Shock-induced damage beneath normal and oblique impact craters (Abstract #1243). In: Lunar and Planetary Science XXXVI

Anderson JLB, Schultz PH, Heineck JT (2003) Asymmetry of ejecta flow during oblique impacts using three-dimensional particle image velocimetry. J Geophys Res Planets 108:1–10. https://doi.org/10.1029/2003je002075

Anderson JLB, Schultz PH, Heineck JT (2004) Experimental ejection angles for oblique impacts: Implications for the subsurface flow-field. Meteorit Planet Sci 39:303–320. https://doi.org/10.1111/j.1945-5100.2004.tb00342.x

Basu AK (1986) Geology of parts of the Bundelkhand Granite Massif, Central India. Records Geol Surv India 117:61–124

Bhatt SC, Singh VK (2011) Implications of shear indicators for tectonic evolution of Mauranipur shear zone, Bundelkhand craton, central India. In: 2nd International Conference, Precambrian Continental Growth and Tectonism. pp 36–49

Bottke WF, Love SG, Tytell D, Glotch T (2000) Interpreting the elliptical crater populations on mars, venus, and the moon. Icarus 145:108–121. https://doi.org/10.1006/icar.1999.6323

Buhl E, Kowitz A, Elbeshausen D et al (2013a) Particle size distribution and strain rate attenuation in hypervelocity impact and shock recovery experiments. J Struct Geol 56:20–33. https://doi.org/10.1016/J.JSG.2013.08.007

Buhl E, Poelchau MH, Dresen G, Kenkmann T (2013b) Deformation of dry and wet sandstone targets during hypervelocity impact experiments, as revealed from the MEMIN program. Meteorit Planet Sci 48:71–86. https://doi.org/10.1111/j.1945-5100.2012.01431.x

Buhl E, Poelchau M, Dresen G, Kenkmann T (2014) Scaling of sub-surface deformation in hypervelocity impact experiments on porous sandstone. Tectonophysics 634:171–181. https://doi.org/10.1016/j.tecto.2014.07.030

Burcheil MJ, Mackay NG (1998) Crater ellipticity in hypervelocity impacts on metals. J Geophys Res 103:22761–22774

Collins GS, Patel N, Davison TM et al (2020) A steeply-inclined trajectory for the Chicxulub impact. Nat Commun 11:1–10. https://doi.org/10.1038/s41467-020-15269-x

Dahl JM, Schultz PH (2001) Measurement of stress wave asymmetries in hypervelocity projectile impact experiments. Int J Impact Eng 26:145–155. https://doi.org/10.1016/S0734-743X(01)00077-X

Davison TM, Collins GS (2022) Complex crater formation by oblique impacts on the earth and moon. Geophys Res Lett 49:1–9. https://doi.org/10.1029/2022GL101117

Davison TM, Collins GS, Elbeshausen D et al (2011) Numerical modeling of oblique hypervelocity impacts on strong ductile targets. Meteorit Planet Sci 46:1510–1524. https://doi.org/10.1111/j.1945-5100.2011.01246.x

Deb T, Bhattacharyya T (2022) The evolution of the fracture systems under progressive sinistral shear in the Bundelkhand Craton a review and new insights. Earth Sci Rev Central India. https://doi.org/10.1016/j.earscirev.2022.104238

Dershowitz WS, Herda HH (1993) Interpretation of fracture spacing and intensity. In: International Journal of Rock Mechanics and Mining Sciences & Geomechanics Abstracts. Pergamon, pp 757–766

Duvall AR, Harbert SA, Upton P et al (2020) River patterns reveal two stages of landscape evolution at an oblique convergent margin, Marlborough Fault System, New Zealand. Earth Surf Dyn 8:177–194. https://doi.org/10.5194/esurf-8-177-2020

Ekholm AG, Melosh HJ (2001) Crater features diagnostic of oblique impacts: the size and position of the central peak. Geophys Res Lett 28:623–626. https://doi.org/10.1029/2000GL011989

Elbeshausen D, Wünnemann K, Collins GS (2009) Scaling of oblique impacts in frictional targets: Implications for crater size and formation mechanisms. Icarus 204:716–731. https://doi.org/10.1016/j.icarus.2009.07.018

Elbeshausen D, Wünnemann K, Collins GS (2013) The transition from circular to elliptical impact craters. J Geophys Res Planets 118:2295–2309. https://doi.org/10.1002/2013JE004477

Field JE (1971) Brittle fracture: Its study and application. Contemp Phys 12:1–31. https://doi.org/10.1080/00107517108205103

Gault DE, Wedekind JA (1978) Experimental studies of oblique impact. Lunar Planet Sci Conf Proc 3:3843–3975
Gerrard AJ (1988) Rocks and landforms, 1st edn. Springer, Dordrecht
Gilbert GK (1893) The moon's face: a study of the origin of its features. Harvard University Press, Cambridge
Goltrant O, Leroux H, Doukhan JC, Cordier P (1992) Formation mechanisms of planar deformation features in naturally shocked quartz. Phys Earth Planet Inter 74:219–240. https://doi.org/10.1016/0031-9201(92)90012-K
Heineck JT, Schultz PH, Anderson JLB (2002) Application of three-component PIV to the measurement of hypervelocity impact ejecta. J vis (tokyo) 5:233–241. https://doi.org/10.1007/BF03182331
Herrick RR, Forsberg-Taylor NK (2003) The shape and appearance of craters formed by oblique impact on the moon and venus. Meteorit Planet Sci 38:1551–1578. https://doi.org/10.1111/j.1945-5100.2003.tb00001.x
Joshi G, Phukon P, Agarwal A, Ojha AK (2023) On the emplacement of the impact melt at the Dhala impact structure India. J Geophys Res Planets. https://doi.org/10.1029/2023JE007840
Kenkmann T, Jahn A, Scherler D, Ivanov BA (2005) Structure and formation of a central uplift: a case study at the Upheaval Dome impact crater, Utah. Special Paper Geol Soc Am 384:85–115. https://doi.org/10.1130/0-8137-2384-1.85
Kenkmann T, Poelchau MH, Wulf G (2014) Structural geology of impact craters. J Struct Geol 62:156–182. https://doi.org/10.1016/j.jsg.2014.01.015
Kenkmann T, Wulf G, Agarwal A (2020) Ramgarh, Rajasthan, India: A 10 km diameter complex impact structure. Meteorit Planet Sci 55:936–961. https://doi.org/10.1111/maps.13454
Khorsand Zak A, Majid WHA, Ebrahimizadeh Abrishami M et al (2012) Synthesis, magnetic properties and X-ray analysis of Zn 0.97X 0.03O nanoparticles (X = Mn, Ni, and Co) using Scherrer and size-strain plot methods. Solid State Sci 14:488–494. https://doi.org/10.1016/j.solidstatesciences.2012.01.019
Kibasomba PM, Dhlamini S, Maaza M et al (2018) Strain and grain size of TiO2 nanoparticles from TEM, Raman spectroscopy and XRD: the revisiting of the Williamson-Hall plot method. Results Phys 9:628–635. https://doi.org/10.1016/j.rinp.2018.03.008
Kumar S, Agarwal A, Rae ASP et al (2023) Use of magnetic fabrics and X-ray diffraction to reveal low strains in experimentally deformed Maggia gneiss. Int J Earth Sci 112:867–879. https://doi.org/10.1007/s00531-022-02284-0
Langenhorst F, Deutsch A, Stöffler D, Hornemann U (1992) Effect of temperature on shock metamorphism of single-crystal quartz. Nature 356:507–509. https://doi.org/10.1038/356507a0
Lei Q, Latham J-P, Tsang C-F (2017) The use of discrete fracture networks for modelling coupled geomechanical and hydrological behaviour of fractured rocks. Comput Geotech 85:151–176. https://doi.org/10.1016/j.compgeo.2016.12.024
Lindström M, Shuvalov V, Ivanov B (2005) Lockne crater as a result of marine-target oblique impact. Planet Space Sci 53:803–815. https://doi.org/10.1016/j.pss.2005.02.005
Malviya VP, Arima M, Pati JK, Kaneko Y (2006) Petrology and geochemistry of metamorphosed basaltic pillow lava and basaltic komatiite in the Mauranipur area: Subduction related volcanism in the Archean Bundelkhand craton, Central India. J Mineral Petrol Sci 101:199–217. https://doi.org/10.2465/jmps.101.199
Michikami T, Hagermann A, Morota T et al (2017) Oblique impact cratering experiments in brittle targets: Implications for elliptical craters on the moon. Planet Space Sci 135:27–36. https://doi.org/10.1016/j.pss.2016.11.004
Molnar P, Anderson RS, Anderson SP (2007) Tectonics, fracturing of rock, and erosion. J Geophys Res Earth Surf 112:1–12. https://doi.org/10.1029/2005JF000433
Mondal MEA, Goswami JN, Deomurari MP, Sharma KK (2002) Ion microprobe 207 Pb/ 206 Pb ages of zircons from the Bundelkhand massif, northern India: implications for crustal evolution of the Bundelkhand-Aravalli protocontinent. Precambr Res. https://doi.org/10.1016/S0301-9268(02)00078-5
Monecke T, Kempe U, Gotze J (2002) Genetic signi¢cance of the trace element content in metamorphic and hydrothermal quartz: a reconnaissance study. Earth Planet Sci Lett 202:709–724
Nasiri-Tabrizi B (2014) Thermal treatment effect on structural features of mechano-synthesized fluorapatite-titania nanocomposite: a comparative study. J Adv Ceram 3:31–42. https://doi.org/10.1007/s40145-014-0090-4
Nesse WD (2017) Introduction to mineralogy, 3rd edn. Oxford University Press, Oxford
Pati JK, Reimold WU, Koeberl C, Pati P (2008) The Dhala structure, Bundelkhand craton, Central India—eroded remnant of a large paleoproterozoic impact structure. Meteorit Planet Sci 43:1383–1398. https://doi.org/10.1111/j.1945-5100.2008.tb00704.x
Pati JK, Jourdan F, Armstrong RA et al (2010) First SHRIMP U-Pb and 40 Ar/ 39 Ar chronological results from impact melt breccia from the Paleoproterozoic Dhala impact structure, India. Special Paper Geol Soc Am 465:571–591. https://doi.org/10.1130/2010.2465(27)
Pati JK, Reimold WU, Greshake A et al (2015) Pseudotachylitic breccia from the Dhala impact structure, north-central India: texture, mineralogy and geochemical characterization. Tectonophysics 649:18–32. https://doi.org/10.1016/j.tecto.2015.01.021
Pati JK, Poelchau MH, Reimold WU et al (2019) Documentation of shock features in impactites from the Dhala impact structure, India. Meteorit Planet Sci 54:2312–2333. https://doi.org/10.1111/maps.13369
Pierazzo E, Melosh HJ (1999) Hydrocode modeling of Chicxulub as an oblique impact event. Earth Planet Sci Lett 165:163–176. https://doi.org/10.1016/S0012-821X(98)00263-5
Pierazzo E, Melosh HJ (2000a) Understanding oblique impacts from experiments, observations, and modelling. Annu Rev Earth Planet Sci 28:141–167. https://doi.org/10.1146/annurev.earth.28.1.141
Pierazzo E, Melosh HJ (2000b) Hydrocode modeling of oblique impacts: the fate of the projectile. Meteorit Planet Sci 35:117–130. https://doi.org/10.1111/j.1945-5100.2000.tb01979.x
Poelchau MH, Kenkmann T (2008) Asymmetric signatures in simple craters as an indicator for an oblique impact direction. Meteorit Planet Sci 43:2059–2072. https://doi.org/10.1111/j.1945-5100.2008.tb00661.x
Prasad MH, Hakim A, Rao BK (1999) Metavolcanic and metasedimentary inclusions in the Bundelkhand granitic complex in Tikamgarh district, Madhya Pradesh. J Geol Soc India 54:359–368
Reznik B, Kontny A, Fritz J, Gerhards U (2016) Shock-induced deformation phenomena in magnetite and their consequences on magnetic properties. Geochem Geophys Geosyst 17:2374–2393. https://doi.org/10.1002/2016GC006338
Rogers S, Bewick R, Brzovic A, Gaudreau D (2017) Integrating photogrammetry and discrete fracture network modelling for improved conditional simulation of underground wedge stability. In: Proceedings of the Eighth International Conference on Deep and High Stress Mining. Australian Centre for Geomechanics. Perth
Roy SG, Koons PO, Upton P, Tucker GE (2015) The influence of crustal strength fields on the patterns and rates of fluvial incision. J Geophys Res Earth Surf. https://doi.org/10.1002/2014JF003281
Roy SG, Tucker GE, Koons PO et al (2016) A fault runs through it: modeling the influence of rock strength and grain-size distribution in a fault-damaged landscape. J Geophys Res Earth Surf. https://doi.org/10.1002/2015JF003662
Saha L, Pant NC, Pati JK et al (2011) Neoarchean high-pressure margarite-phengitic muscovite-chlorite corona mantled corundum in quartz-free high-Mg, Al phlogopite-chlorite schists from the Bundelkhand craton, north central India. Contrib Miner Petrol 161:511–530. https://doi.org/10.1007/s00410-010-0546-7
Sarangi S, Gopalan K, Kumar S (2004) Pb-Pb age of earliest megascopic, eukaryotic alga bearing Rohtas formation, vindhyan supergroup, india: implications for precambrian atmospheric oxygen evolution. Precambrian Res 132:107–121. https://doi.org/10.1016/j.precamres.2004.02.006
Schultz PH, Anderson RR (1996) Asymmetry of the Manson impact structure: evidence for impact angle and direction. Geol Soc Am Spec Pap 302:7
Schultz PH, D'Hondt S (1996) Cretaceous-tertiary (Chicxulub) impact angle and its consequences. Geology 24:963–967
Shoemaker EM, Shoemaker CS (1996) The proterozoic impact record of Australia. AGSO J Aust Geol Geophys 16:379–398
Shuvalov V (2011) Ejecta deposition after oblique impacts: an influence of impact scale. Meteorit Planet Sci 46:1713–1718. https://doi.org/10.1111/j.1945-5100.2011.01259.x
Singh AK, Pati JK, Sinha R et al (2021) Characteristic landforms and geomorphic features associated with impact structures: observations at the

Dhala structure, north-central India. Earth Surf Process Landf 46:1482–1503. https://doi.org/10.1002/esp.5115
Stöffler D, Langenhorst F (1994) Shock metamorphism of quartz in nature and experiment: I. basic observation and theory*. Meteoritics 29:155–181
Stöffler D, Gault DE, Wedekind J, Polkowski G (1975) Experimental hypervelocity impact into quartz sand: distribution and shock metamorphism of ejecta. J Geophys Res 80:4062–4077. https://doi.org/10.1029/JB080i029p04062
Stöffler D, Artemieva NA, Pierazzo E (2002) Modeling the Ries-Steinheim impact event and the formation of the moldavite strewn field. Meteorit Planet Sci 37:1893–1907. https://doi.org/10.1111/j.1945-5100.2002.tb01171.x
Stöffler D, Hamann C, Metzler K (2017) Shock metamorphism of planetary silicate rocks and sediments: proposal for an updated classification system. Meteorit Planet Sci 53:5–49. https://doi.org/10.1111/maps.12912
Sugandhi E, Agarwal A (2022) Jet onset time and velocity for various natural hypervelocity impacts. Int J Impact Eng. https://doi.org/10.1016/j.ijimpeng.2022.104310
Sugandhi E, Agarwal A, Saha A, Joshi G (2024) Effects of Hugoniot properties on jet onset conditions. Int J Impact Eng 188:104930. https://doi.org/10.1016/j.ijimpeng.2024.104930
Thandavan TMK, Gani SMA, Wong CS, Nor RM (2015) Evaluation of Williamson-hall strain and stress distribution in ZnO nanowires prepared using aliphatic alcohol. J Nondestr Eval 34:1–9. https://doi.org/10.1007/s10921-015-0286-8
Tonkins MC, Coggan JS (2017) Characterization of Rock Fracturing for Vertical Boreability. Procedia Engineering Elsevier Ltd., Philadelphia
Tsikalas F (2005) Mjølnir crater as a result of oblique impact: asymmetry evidence constrains impact direction and angle impact tectonics. Springer-Verlag, Berlin
Ungár T (2004) Microstructural parameters from X-ray diffraction peak broadening. Scr Mater 51:777–781. https://doi.org/10.1016/j.scriptamat.2004.05.007
Wallis D, Burchell MJ, Cook AC et al (2005) Azimuthal impact directions from oblique impact crater morphology. Mon Not R Astron Soc 359:1137–1149. https://doi.org/10.1111/j.1365-2966.2005.08978.x
Williamson GK, Hall WH (1953) X-ray line broadening from filed aluminium and wolfram. Acta Metall 1:22–31. https://doi.org/10.1016/0001-6160(53)90006-6
Wu Y, Chen Z, Nan P et al (2019) Lattice strain advances thermoelectrics. Joule 3:1276–1288. https://doi.org/10.1016/j.joule.2019.02.008

Publisher's Note